Maternal RND3/RhoE deficiency impairs placental mitochondrial function in preeclampsia by modulating the PPARγ-UCP2 cascade

Liping Huang[1 †], Yanlin Ma[2 †], Lu Chen[1], Jiang Chang[3], Mei Zhong[1], Zhijian Wang[1], Ying Sun[4], Xia Chen[1], Fei Sun[1], Lu Xiao[1], Jianing Chen[1], Yingjun Lai[1], Chuming Yan[1], Xiaojing Yue[1 *]

1. Department of Obstetrics and Gynecology, Nanfang Hospital, Southern Medical University, Guangzhou, China.
2. Hainan Provincial Key Laboratory for Human Reproductive Medicine and Genetic Research, Reproductive Medical Center, The First Affiliated Hospital of Hainan Medical University, Hainan Medical University, Haikou, China
3. Institute of Biosciences and Technology, Texas A&M University Health Science Center, Houston, US.
4. Department of Obstetrics and Gynecology, Affiliated Shenzhen Maternity and Child Healthcare Hospital, Southern Medical University, Shenzhen, China

Running title: Rnd3 regulates mitochondria in preeclampsia

***Correspondence to**: Xiaojing Yue, PhD (yuexj1986@163.com);
Phone: (86) 020-62787551
Mailing address: Southern Medical University, 1023 South Shatai Rd, Guangzhou 510515, China.

†These authors contributed equally to this work.

Word count

Abstract: 162 words

Article length: 4302 words

Abbreviations

ACOG, American College of Obstetricians and Gynecologists; CK7, cytokeratin 7; CTB, cytotrophoblast; DHE, dihydroethidium; FBS, fetal bovine serum; IUGR, fetal intrauterine growth restriction; LOC, loss of cristae; NRF1, nuclear respiratory factor 1; OCR, oxygen consumption rates; PE, preeclampsia; PGC1-α, PPARγ coactivator 1-α; PPARα, peroxisome proliferator-activated receptor α; PPARγ, peroxisome proliferators-activated receptor γ; PTBs, primary trophoblasts; ROS, reactive oxygen species; SOD1, superoxide dismutase 1; SOD2, superoxide dismutase 2; STB, syncytiotrophoblast; TFAM, mitochondrial transcription factor A; TUNEL, terminal deoxynucleotidyl transferase dUTP nick end labeling; UCP2, mitochondrial uncoupling protein 2.

Abstract

Preeclampsia (PE) is a life-threatening disease of pregnant women associated with severe hypertension, proteinuria, or multi-organ injuries. Mitochondrial-mediated placental oxidative stress plays a key role in the pathogenesis of PE. However, the underlying mechanism remains to be revealed. Here, we identify Rnd3, a small Rho GTPase, regulating placental mitochondrial reactive oxygen species (ROS). We showed that Rnd3 is down-regulated in primary trophoblasts isolated from PE patients. Loss of Rnd3 in trophoblasts resulted in excessive ROS generation, cell apoptosis, mitochondrial injury, and proton leakage from the respiratory chain. Moreover, Rnd3 overexpression partially rescues the mitochondrial defects and oxidative stress in human PE primary trophoblasts. Rnd3 physically interacts with the peroxisome proliferators-activated receptor γ (PPARγ) and promotes the PPARγ-mitochondrial uncoupling protein 2 (UCP2) cascade. Forced expression of PPARγ rescues deficiency of Rnd3-mediated mitochondrial dysfunction. We conclude that Rnd3 acts as a novel protective factor in placental mitochondria through PPARγ-UCP2 signaling and highlight that downregulation of Rnd3 is a potential factor involved in PE pathogenesis.

Keywords: Rnd3, Preeclampsia, Mitochondrion, Oxidative stress, PPARγ

Introduction

Preeclampsia (PE) is a pregnancy complication that occurs after the 20th gestational week and is characterized by maternal hypertension, proteinuria, and multi-organ injuries. It affects 5-7% of pregnancies and is the leading cause of perinatal morbidity and mortality(1). Most of the cases with PE are associated with fetal intrauterine growth restriction (IUGR) and a high risk of maternal cardiovascular disease later in life(2). Although the mechanisms responsible for PE's pathogenesis have not been entirely clarified, placental oxidative stress and poor vascularization are thought to be its leading cause(2, 3). Oxidative stress is generated by the imbalance of reactive oxygen species (ROS) and the endogenous oxidant scavenging system(4). Excessive ROS accumulation is identified in PE pathogenesis as the contributor to endothelial dysfunction and placental inflammation response(5-7). Although the shallow invasion of trophoblasts to decidua and subsequently failed spiral artery remodeling participate in placental ischemia and oxidative stress, accumulating evidence has shown that mitochondrial dysfunction during PE also can induce an increase in the level of ROS and cause placental oxidative stress(8-10). Abnormalities in mitochondria' morphology, including swelling mass and disappearance of cristae, have been observed in trophoblasts of PE placenta(11). However, a limited number of studies have investigated the molecular machinery of the mitochondrial ROS during PE.

Peroxisome proliferators-activated receptor γ (PPARγ) is a ligand-inducible transcription factor that plays critical roles in mitochondrial biogenesis, dynamics, and metabolism(12, 13). Loss of PPARγ in a mouse model caused embryonic lethality with major placental defects(14) due to its critical roles in placental vasculature and the differentiation of complicated trophoblast lineages(15-17). Recent studies have revealed that the circulating agonists' levels of PPARγ were significantly reduced in PE patients(14, 18). In contrast, administration of rosiglitazone, a selective PPARγ agonist, could largely ameliorate PE in a RUPP-induced PE rat model(19). Nevertheless, the regulatory mechanism of the downregulated PPARγ signaling in PE

130 remains unknown.

131

132 Rnd3 is a small GTPase, also called RhoE, that exhibits multiple regulatory functions
133 in carcinogenesis, cardiovascular diseases, and neural development(20-25). *Rnd3* has
134 been proposed to be a PE candidate gene based on a population study. A specific *Rnd3*
135 SNP (rs115015150) was associated with PE, and several quantitative cardiovascular
136 risk traits(26). Several studies illustrated that Rnd3 was involved with PE and
137 regulating the proliferation, migration, and invasion of trophoblast cells(27-29). In the
138 present study, we identified decreases of Rnd3 expression in placentae and primary
139 trophoblasts from PE patients and indicated a novel protective role of Rnd3 in PE via
140 maintaining mitochondrial function. The possible molecular mechanism is that RND3
141 protein physically interacts with and stabilizes PPARγ. Transcriptionally regulated by
142 PPARγ, uncoupling protein 2 (UCP2) was involved in mitochondrial membrane
143 potential and ROS generation regulation. The downregulated PPARγ-UCP2 cascade
144 was identified and could be reversed by Rnd3 overexpression and rescued
145 mitochondrial dysfunction in human PE primary placental trophoblasts. The findings
146 revealed a new function of Rnd3 in PE and provided new insights into PE
147 pathogenesis.

148

149 **Methods**

150 **Human placental tissues**

151 Human placental tissues were obtained and used for the present study with written
152 patient-informed consent and approval by the Ethics Committee of Southern Hospital,
153 Southern Medical University. PE was defined according to the criteria of the
154 American College of Obstetricians and Gynecologists (ACOG), which required blood
155 pressure ≥ 140/90 mmHg on two occasions at least 4 h apart after 20 weeks of
156 gestation with proteinuria ≥ 0.3 g/24h, or new onset hypertension without proteinuria
157 but with other organ damage, such as thrombocytopenia, kidney or liver dysfunction
158 and pulmonary edema. PE placental tissues were obtained from 24 patients with full
159 term terminated pregnancies with average gestational ages of 36.1 ± 2.8 weeks. The

160 healthy placental tissues were obtained from 34 healthy full term pregnancies with
161 average gestational ages 37.0 ± 1.1 weeks. To ensure that the placental samples were
162 sterile, all placentas were obtained via c-section deliveries consistently. The placental
163 tissues were collected from the mid-section between the chorionic and maternal basal
164 surfaces at four different positions 2 cm from central umbilical cord. Vessels were
165 trimmed from the tissues. Fresh tissue samples were immediately frozen by liquid
166 nitrogen or processed by paraformaldehyde fixation and frozen embedding. Women
167 with a history of smoking and drinking, or diagnosed with multiple gestations, or
168 other complications including chronic hypertension, diabetes, autoimmune and
169 cardiovascular conditions were excluded from the present study. 91.2% PE patients
170 received antihypertensive treatment with Nifedipine (0.5 mg/kg/day) after clinical
171 diagnosis of PE.
172
173 **Electron microscopy analysis**
174 Fresh placental tissue samples were fixed with a buffer containing 2.5%
175 glutaraldehyde (diluted from 25% glutaraldehyde, G5882, Sigma-Aldrich, USA) and
176 were subsequently processed and embedded in LX-112 medium. The ultrathin
177 sections were stained with uranyl acetate and lead citrate, and then were examined in
178 an H-7650 transmission electron microscope (HITACH, Japan).
179
180 **Isolation of primary human trophoblasts**
181 The isolation of primary human trophoblasts was performed as described
182 previously(30). Briefly, the fresh placental tissues were dissected into small pieces
183 and were washed with PBS to remove blood cells. Digestion was performed at 37°C,
184 with the media containing 0.125% trypsin (diluted from 0.25% Trypsin-EDTA, Gibco
185 25200072, USA), 0.03% DNase (D4263, Sigma-Aldrich, USA) and 1%
186 Penicillin-Streptomycin. The digestion were neutralized by 5% fetal bovine serum
187 (FBS). Following five digestion times, the floating cells were harvested by
188 centrifugation at 1,200 x g for 15 min and re-suspended in DMEM medium. The
189 trophoblasts were purified with 5-65% Percoll density gradients (P1644-500 ml,

190 Sigma, USA). The cell surface biomarker cytokeratin 7 (CK7) was used to identify
191 the trophoblasts. A total of 20 immunofluorescent staining images were acquired in
192 different fields by fluorescence microscopy. CK7 positive cells and DAPI-labeled
193 nuclei in each image were counted by the LAS V4.0 software. The trophoblasts' purity
194 was determined by the ratio of the number of CK7 positive cells over that of the total
195 cells.
196
197 **Cell culture and hypoxia treatment**
198 Human primary trophoblasts were cultured in RPMI-1640 medium containing 10%
199 fetal bovine serum (FBS) and 1% Penicillin-Streptomycin. BeWo cells (ATCC
200 CCL-98, USA) were cultured in F-12K medium containing 2 mM Glutamine, 10%
201 FBS, and 1% Penicillin-Streptomycin. The cells were maintained at 37°C with 5%
202 CO_2. Hypoxic cell culture was performed in a hypoxic chamber (MIC-101,
203 Billups-Rothenberg Inc, CA, USA) with 1% O_2 for 16 h.
204
205 **Expression vectors and adenoviral expression vectors**
206 The human Rnd3 cDNA subcloning was performed to generate the expression vectors
207 GFP-RND3 and Myc-RND3 as described previously(22, 24). Human PPARγ cDNA
208 was subcloned into GV141 backbone (GeneChem, Shanghai, China) to generate the
209 expression vector Flag-PPARγ. The AdMax^{TM} system was used for the generation of
210 recombinant adenovirus carrying human *Rnd3* cDNA. Briefly, CMV-EGFP-Rnd3 and
211 viral backbone plasmid pBHG were co-transfected into HEK293 cells, and
212 subsequently, the recombinant adenoviruses were harvested and amplified in HEK293
213 cells.
214
215 **Mitochondrial respiratory function measurement**
216 Mitochondrial respirations were measured at 37°C in a Seahorse XF24 Extracellular
217 Flux Analyzer (Agilent, USA). The XF Cell Mito Stress Test Kit (103015-100,
218 Agilent, USA) and XF24 FluxPak mini (102342-100, Agilent, USA) cartridge were
219 used to determine mitochondrial oxygen consumption rates (OCR) in viable cells. The

220 mitochondrial assay medium consisted of XF Base Medium (102353-100, Agilent,
221 USA), 10 mM glucose, 5 mM sodium pyruvate, and 2 mM L-glutamine at pH 7.4.
222 The OCRs were measured by subsequent addition of 2 μM oligomycin, 1 μM FCCP,
223 and 1 μM antimycin A/1 μM rotenone.
224

225 **Reverse transcription and quantitative PCR**

226 The mRNA transcripts were quantified by quantitative PCR analysis, as described
227 previously(22). Total RNA was prepared by TRIzol extraction. The forward and
228 reverse PCR primers (5′ to 3′) were presented as follows: *RND3* (human):
229 CCAGCCAGAAATTATCCAGCA/GAGAACCCGAAGTGTCCCA; *GAPDH*
230 (human): GAGTCAACGGATTTGGTCGT/TTGATTTTGGAGGGATCTCG; *PPARγ*
231 (human): TCCACATTACGAAGACATTCCA/CGACATTCAATTGCCATGAG;
232 *UCP2* (human): TGGGTTCAAGGCCACAGATG/CCATTGTAGAGGCTTCGGGG;
233 *PGC1α* (human):
234 AGCACTTCGGTCATCCCAG/CAGTTTATCACTTTCATCTTCGC; *NRF1* (human):
235 ATGGAGGAACACGGAGTGAC/TCATCAGCTGCTGTGGAGTT; *TFAM* (human):
236 CCGAGGTGGTTTTCATCTGT/CCGCCCTATAAGCATCTTGA; *PPARα* (human):
237 CTGTCTGCTCTGTGGACTCA/AGAACTATCCTCGCCGATGG; *SOD1* (human):
238 TGAAGGTGTGGGGAAGCATT/GTCACATTGCCCAAGTCTCC; *SOD2* (human):
239 TTTTGGGGTATCTGGGCTCC/TCAAAGGAACCAAAGTCACGT. *GAPDH*
240 expression levels were used for qPCR normalization. The expression levels were
241 determined by the $2^{-\Delta\Delta Ct}$ threshold cycle method.
242

243 **Luciferase assay**

244 The luciferase reporter vector with the 1,000 bp promoter of the human *UCP2* gene
245 was generated with a GV238 backbone (GeneChem, Shanghai, China). The luciferase
246 assay was conducted, as described previously(22). Each measurement was repeated
247 three times. All results were normalized according to the co-transfected *Renilla*
248 luciferase enzyme activity (E1910, Promega).
249

250 **Western immunoblotting, immunoprecipitation, and ELISA**

251 The protein samples for western blot analysis were prepared as described
252 previously(22), and the immunoblotting densitometry was quantified by the ImageJ
253 Software (NIH, USA). For immunoprecipitation, 293T cells were co-transfected with
254 myc-Rnd3 and flag-PPARγ expression vectors. The cells were lysed in RIPA lysis
255 buffer containing protease inhibitors. Cell lysates were incubated with protein A/G
256 magnetic beads (88802, Thermo Fisher Scientific, USA) and either mouse IgG
257 (5415S, Cell Signaling Technology, USA) or anti-Myc-Tag antibody at 4°C overnight.
258 The beads were washed with lysis buffer for 4 times and boiled with 4× SDS loading
259 buffer. The samples were analyzed by immunoblotting and identified with an
260 anti-PPARγ primary antibody. We used the conformation-specific secondary antibody
261 to recognize only the primary antibody but not the heavy and light chain of the
262 antibody used for immunoprecipitation.

263

264 The antibodies used for the present study were from the following sources:
265 anti-Cytokeratin 7 (ab9021, Abcam, USA); anti-PPARγ (2443S), anti-UCP2 (89326S),
266 anti-Rnd3 (3664S), anti-Lamin B1 (12586S), anti-Myc-Tag (2276S), and mouse
267 anti-rabbit IgG (Conformation Specific, 5127S) from Cell Signaling Technology,
268 USA. Equal protein loading for immunoblotting was verified by the β-actin blot's
269 intensity (ab8226, Abcam, USA). Concentration of 8-Isoprostane was assessed by the
270 8-isoprostane ELISA Kit (516351, Cayman Chemical, USA).

271

272 **Fluorescence staining**

273 For histological analysis, fresh placental tissues were embedded in the Tissue-Tek
274 O.C.T. Compound (4583, Sakura, USA). Frozen sections were used for
275 dihydroethidium (DHE) staining (D1168, Thermo Fisher Scientific, USA). Cellular
276 JC-1 (T3168, Thermo Fisher Scientific, USA) staining and DHE staining were
277 performed with viable BeWo cells, respectively. TUNEL staining (11684795910,
278 Roche, Germany) was performed in fixed cells for apoptosis detection.

279

280 **Statistical analysis**

281 The data were expressed as the mean ± standard deviation (SD). An unpaired,
282 two-tailed Student's *t*-test was used for two-group comparison. The one-way ANOVA,
283 followed by the Student-Newman-Keuls method, was used for multiple-group
284 comparison. The mRNA transcripts of Rnd3, PPARγ and UCP2 in human placentas
285 were analyzed with F-test and Wilcoxon rank-sum test. All analyses were conducted
286 using GraphPad Prism 8.0 and SAS 9.4. A value of $P<0.05$ was considered for a
287 significant difference.

288

289 **Results**

290 **The expression of Rnd3 is downregulated in human placentae with PE**

291 To investigate the role of Rnd3 in PE, its expression levels were measured in 24
292 human placentae from PE patients and 34 healthy controls. Women with a history of
293 smoking and drinking or diagnosed with chronic hypertension or gestational diabetes
294 mellitus were excluded from the present study. The clinical characteristics of all
295 pregnant women were presented in Table 1. Clinical data of blood pressure, BMI and
296 proteinuria was collected at the time of PE diagnosis. In the placentae with PE, a
297 62.9% decrease was noted in the RND3 protein levels (Fig.1A), and a 46.0% decrease
298 was reported in the *Rnd3* mRNA level (Fig. 1B). This clinical observation suggested
299 that Rnd3 may act as a potential regulator in the pathogenesis of PE.

300

301 **RND3 protein expression is downregulated in human PE primary trophoblasts**
302 **and is associated with severe oxidative stress and apoptosis**

303 Oxidative stress is the main regulator of PE development. Severe oxidative stress was
304 noted in the placental tissue sections in the human placentae with PE (Fig. 2A).
305 Systemic experiments based on primary human trophoblasts (PTBs) were conducted
306 to understand the underlying mechanisms involved in this process. Human PTBs were
307 isolated from PE and healthy placentas. The PTBs were identified by immunostaining
308 the surface marker cytokeratin 7 (CK7) (Fig. 2B). According to nuclear
309 counterstaining, the purity of the isolated PTBs was 97% (Fig. 2B). The protein level

310 of RND3 in the PTBs was detected by immunostaining analysis. Rnd3 was
311 universally expressed in the cytoplasm and nuclei of the trophoblasts (Fig 2C).
312 Reduced Rnd3 expression was associated with increased ROS accumulation and was
313 detected in the PE patient-derived PTBs (Fig 2C). To mimic the pathological PE
314 placental environment, hypoxic cell culture of PTBs was established. Following
315 hypoxia induction, additional ROS accumulation and apoptosis were observed in the
316 PE PTBs compared with those noted in control PTBs (Fig 2D). This suggested that
317 PE PTBs were more sensitive to hypoxic stress. Rnd3 may participate in the
318 development of PE via the regulation of ROS generation.
319

320 **Human PE primary placental trophoblasts are predisposed to mitochondrial**
321 **damage**

322 To explore the underlying mechanism of Rnd3-associated oxidative stress in PE,
323 trophoblastic mitochondria, which are the main source of ROS, were analyzed by
324 electron microscopy. In the placental tissues' ultrathin sections, a borderline between
325 the layers of syncytiotrophoblast (STB) and cytotrophoblast (CTB) could be
326 identified. In the STB of the PE placentae, swelling mitochondria with loss of cristae
327 (LOC) were observed, which were the typical characteristics of mitochondrial damage
328 (arrows pointed, Fig 3A). We further analyzed the mitochondrial membrane potential
329 in PTBs. Using JC1 staining, we compared the mitochondrial membrane potential
330 between the control PTBs and the PE PTBs with or without hypoxic stimuli. The JC1
331 red/green fluorescence ratios between the two groups indicated no difference at the
332 baseline (Fig 3B). The mitochondrial membrane potential was reduced in response to
333 the hypoxic challenge. However, the red/green fluorescence emission ratio was
334 collapsed in PE PTBs compared with that noted in control PTBs (Fig 3B), indicating
335 that PE PTBs were predisposed to hypoxia-induced mitochondrial injury.
336

337 **Overexpression of Rnd3 protects the trophoblastic cells from ROS generation**
338 **and induction of apoptosis**

339 To investigate the potential role of Rnd3 deficiency in inducing oxidative stress in PE

340 PTBs, we manipulated Rnd3 expression in the trophoblastic BeWo cell line. Hypoxic
341 cell culture was applied to induce ROS generation. ROS levels were determined by
342 DHE fluorescence labeling and the detection of cellular 8-isoprostane levels. The
343 GFP-Rnd3 expressing BeWo cells displayed significantly decreased ROS levels than
344 those of the surrounding non-GFP-Rnd3 cells (Fig 4A). Consistent with these
345 observations, myc-Rnd3 overexpression led to decreased 8-isoprostane levels (Fig 4B)
346 and ameliorated cell apoptosis (Fig 4C-D), indicating that Rnd3 modulated the
347 production of ROS in trophoblasts. Rnd3 deficiency was observed in human PE PTBs
348 and may cause severe oxidative stress and apoptosis in PE.
349
350 **Rnd3 deficiency leads to mitochondrial damage in BeWo trophoblastic cells**
351 To investigate if mitochondria contributed to Rnd3-mediated ROS generation, we
352 knocked down Rnd3 in BeWo cells. Electron microscopy of Rnd3 knockdown BeWo
353 cells revealed the mitochondrial injury. The compromised mitochondria displayed a
354 structure with loss of cristae (LOC) and swelling mass (arrow pointed, Fig 5A).
355 Consistent with the morphological changes, the mitochondrial transmembrane
356 potential was also depolarized following Rnd3 knockdown (Fig 5B). Subsequently,
357 the effects of Rnd3 on mitochondrial function were assessed by measuring the oxygen
358 consumption rate (OCR) in different respiratory states. Comparing the Rnd3
359 knockdown group and the control group indicated no significant differences in the
360 OCR of the basal respiration, maximal respiration, and space capacity (Fig 5C).
361 However, a 2.4-fold increase in the proton leak associated OCR has detected in the
362 Rnd3 knockdown BeWo cells (Fig 5C), indicating the uncoupling of ATP synthesis
363 and substrate oxidation. Consistent with this result, the mitochondrial coupling
364 efficiency was reduced in the siRnd3 group (Fig 5D).
365
366 **Rnd3 facilitates the protein accumulation of PPARγ and stimulates the**
367 **expression of UCP2 in trophoblasts**
368 To explore the mechanisms of Rnd3-mediated mitochondrial dysfunction, the mRNA
369 expression levels of the mitochondrial regulatory factors and ROS scavengers were

370 evaluated in siRnd3 transiently transfected BeWo cells. The analysis indicated no
371 significant difference between siRnd3 and control groups with regard to the mRNA
372 levels of the transcription factors *PPARγ*, *PPARγ* coactivator 1-α (*PGC1-α*),
373 peroxisome proliferator-activated receptor α (*PPARα*), nuclear respiratory factor 1
374 (*NRF1*), and mitochondrial transcription factor A (*TFAM*) (Fig S1). No significant
375 differences were also noted about the levels of the endogenous ROS scavenger
376 superoxide dismutase 1 (SOD1) and superoxide dismutase 2 (SOD2) (Fig S1).
377
378 Mitochondrial uncoupling protein 2 (UCP2) is critical for mitochondrial respiratory
379 coupling. Rnd3 promoted the protein and the mRNA expression levels of *UCP2*,
380 whereas knockdown of Rnd3 resulted in UCP2 deficiency (Fig 6A-6C), which was
381 consistent with the mitochondrial respiratory coupling defect in siRnd3-transfected
382 cells. As PPARγ has been identified as a transcriptional regulator of UCP2(31), we
383 next assessed its expression levels. It is interesting to note that although the mRNA
384 transcripts of PPARγ did not change the following manipulation of *Rnd3* (Fig S1), the
385 PPARγ protein expression was stimulated by myc-Rnd3 overexpression and was
386 repressed by Rnd3 knockdown (Fig 6A-6B), suggesting a possible post-translational
387 regulation of PPARγ by Rnd3.
388
389 **RND3 is physically bound to PPARγ and results in the accumulation of PPARγ in**
390 **the nuclei**
391 To investigate if Rnd3 could functionally regulate PPARγ protein, we knocked down
392 and overexpressed the latter in BeWo cell cultures. As a transcription factor, the
393 nuclear distribution of PPARγ is critical for maintaining its biological function. We
394 detected apparent nuclear accumulation of PPARγ protein corresponding to the
395 increase in Rnd3 expression. The opposite trend was observed when Rnd3 was
396 knocked down (Fig 6D). Subsequently, a luciferase experiment was conducted to
397 determine if Rnd3 caused any effect on its transcriptional activity. The luciferase
398 reporter was driven by a *UCP2* promoter, which was responsible for the
399 PPARγ-dependent transcriptional activity. Myc-Rnd3 overexpression resulted in a

400 5.2-fold increase in luciferase activity compared with that of the control, while
401 downregulation of Rnd3 weakened PPARγ transcriptional activity and resulted in a
402 68% declined luciferase signal (Fig 6E). To further explore the potential mechanism
403 of Rnd3-induced PPARγ protein accumulation, we performed an *in vivo*
404 coimmunoprecipitation assay with 293T cells. As shown in Fig 6F, physical
405 interaction between Myc-RND3 and Flag-PPARγ proteins was detected. Moreover,
406 we performed co-immunostaining of these two proteins in BeWo cells and confirmed
407 the co-localization of RND3 and PPARγ protein molecules and the reduced nuclear
408 PPARγ protein levels in Rnd3 knockdown cells (Fig 6G).
409

410 **Mitochondrial dysfunction mediated by Rnd3 deficiency is attenuated by PPARγ**
411 **overexpression**

412 To assess whether PPARγ downregulation is responsible for Rnd3 deficiency-induced
413 mitochondrial defects, Flag-PPARγ was overexpressed in Rnd3 knockdown BeWo
414 cells. The improvement in mitochondrial membrane potential and mitochondrial
415 morphological integrity was observed following PPARγ overexpression (Fig 7A-C).
416 The ROS levels were detected by DHE labeling. We also detected 8-isopropane levels.
417 PPARγ overexpression further ameliorated Rnd3 deficiency-mediated oxidative stress
418 (Fig 7D-F). We analyzed the expression levels of UCP2 in Rnd3 knockdown BeWo
419 cells with or without administration of Flag-PPARγ. As expected, PPARγ attenuated
420 Rnd3 deficiency-induced UCP2 downregulation both at the mRNA and protein levels
421 (Fig 7G-H). Finally, we assessed the mitochondrial respiratory functions of the
422 different groups of BeWo cells. Overexpression of PPARγ significantly protected the
423 mitochondrial function with improved proton leakage and coupler efficiency (Fig
424 7I-J).
425

426 **Adenoviral-mediated Rnd3 overexpression in human PE primary trophoblasts**
427 **rescues oxidative stress and mitochondrial defect**

428 Rnd3 downregulation was demonstrated in human PE-PTBs along with severe
429 oxidative stress and mitochondrial injury. To further reveal the critical role of Rnd3 in

430 the clinical pathology of PE, we overexpressed hRnd3 in human PTBs by
431 adenoviral-mediated gene delivery. Elevated RND3 protein levels in Ad-GFP-hRnd3
432 treated PTBs were confirmed by western blot analysis (Fig 8D). In the absence of
433 Ad-GFP-hRnd3 infection, the baseline PE-PTBs exhibited higher ROS levels
434 compared with those of the control-PTBs (Fig 8A, cells displaying no GFP, pointed
435 by long arrows). Following infection with Ad-GFP-hRnd3, the ROS levels of the
436 PE-PTBs were significantly reduced (Fig 8A, cells expressing GFP, indicated by
437 arrowheads). The levels of 8-isopropane were decreased in PE-PTBs following
438 Ad-GFP-hRnd3 application (Fig 8B), which was consistent with the previous
439 observations. Increased expression levels of PPARγ and UCP2 were observed, as
440 expected, in the PTBs with Ad-GFP-hRnd3 (Fig 8C-D). In addition to regulating the
441 PPARγ/UCP2 pathway, Rnd3 further attenuated the mitochondrial function in
442 PE-PTBs (Fig 8E-G).
443

444 **Downregulation of the expression levels of PPARγ and UCP2 were observed in**
445 **human placentae with PE**

446 The expression levels of PPARγ and UCP2 were evaluated in human PE placental
447 tissues. The experiments aimed to offer additional insight into the clinical relevance of
448 regulating the PPARγ/UCP2 pathway by Rnd3 in PE. PPARγ protein levels were
449 downregulated in PE placentae. Consistent with the post-transcriptional regulation of
450 PPARγ by Rnd3, the corresponding mRNA levels of *PPARγ* indicated no significant
451 changes between the control and PE groups (Fig 9A-B). The mRNA transcripts of
452 *UCP2* and its protein levels were reduced in human PE placentae (Fig 9A and C).
453

454 **Discussion**

455 PE has been suggested as a mitochondrial disorder since the late 1980s(32). Proteome
456 analysis of PE placentae revealed that the abnormal expression of the respiratory
457 complex proteins was associated with ROS's excessive generation in the
458 mitochondrial respiratory chain(33). Given that mitochondrial ROS is an important
459 contributor to oxidative stress and inflammation, the reason causing placental

460 mitochondrial ROS is critical and remains to be revealed. This study uncovers a novel
461 understanding of placental oxidative stress in PE that Rnd3-mediated PPARγ/UCP2
462 cascade participates in mitochondrial dysfunction regulation.
463
464 In PE's pathological condition, Rnd3 promotes trophoblasts' proliferation and
465 migration under regulations by lncRNAs HOXA11-AS and TUG1(27, 28). In contrast
466 to these observations, Rnd3 has also been proposed as a stimulator of trophoblast cell
467 invasion in PE, under the repression caused by miR-182-5p(29). Our study confirmed
468 the regulatory role of Rnd3 in PE and revealed the novel function of Rnd3 in
469 maintaining the mitochondrial respiratory chain. The supply of Rnd3 in PE
470 patient-derived primary trophoblasts significantly improved mitochondrial function
471 and repressed oxidative stress (Fig 8), suggesting the potential role of Rnd3 as a
472 pharmacological target for PE.
473
474 Reductions in *Rnd3* mRNA and protein levels were observed in human PE placentas.
475 One possible factor regulating Rnd3 expression could be hypoxia. In BeWo cells, the
476 expression of Rnd3 was stimulated by cAMP/PKA signaling, however, was inhibited
477 under hypoxic condition(34). These suggest that, in PE pathogenesis, failed spiral
478 artery remodeling causes placental ischemia and hypoxia, and thereby contributing to
479 the downregulation of Rnd3 in placenta. Moreover, IGFBP1 was found
480 downregulated in the serum of women with PE, and the downregulation of IGFBP1
481 may participated in pathogenesis of PE by hindering trophoblast migration through
482 ROCK1 and ROCK2 pathway(35). Considering that ROCK1 phosphorylates and
483 stabilizes RND3 protein, these may explain the reduce of Rnd3 in PE patients(36).
484
485 Sun's group reported increases in the mRNA levels of *Rnd3* in the placentas from PE
486 patients, which is opposite to our data(27, 28). To verify the expression pattern of
487 Rnd3 in PE, we detected both mRNA and protein expressions of Rnd3, and confirmed
488 the downregulation of Rnd3 in the PE placentas. One reason of the controversy could
489 be that the specimens were obtained at different sites of placentas. Sun's group

490 collected placental tissue samples from the central area of the placenta's maternal
491 surface(27). In our study, the placental tissues were collected from the mid-section
492 between the chorionic and maternal basal surfaces at four different positions 2 cm
493 from central umbilical cord. The distribution of villous structure within placenta is
494 variable. Cytotrophoblasts and syncytiotrophoblasts cover the surface of villi, and
495 therefore the tissues from placenta's maternal surface consist of large amount of
496 trophoblasts. Whereas the tissues between the chorionic and maternal surfaces were
497 more likely consist of villous core stroma, including mesenchymal cells, hofbauer
498 cells and fibroblasts, as well as trophoblastic layers. Meanwhile, blood vessels were
499 also non-uniformly distributed, with main branches enriched in the central area of
500 placenta. Therefore, the protein expressions from different sites of placentas were
501 highly variable. Besides, samples were obtained at different gestation weeks (33.93 ±
502 3.231, n=60 vs. 36.1 ± 2.8, n=24; p=0.005), which may also contribute to the
503 difference in Rnd3 expressions.
504
505 UCP2 exerts protective properties against oxidative damage by reducing ROS
506 generation via decreasing mitochondrial proton gradient and local oxygen
507 availability(37). PPARγ and its ligands directly activate the *UCP2* gene promoter via
508 the E-box element(31). By recovering the mitochondrial membrane potential and
509 reducing ROS generation, PPARγ improves trophoblast cells' survival under hypoxic
510 conditions (38). In the present study, reduced PPARγ/UCP2 signaling was detected in
511 human PE placentas, contributing to mitochondrial defect and oxidative stress in PE
512 primary trophoblasts. However, excessive stimulation of PPARγ/UCP2 has also been
513 implicated in pathological placenta with maternal nutrient restriction by enhancing
514 fatty acid metabolism and limiting glucose utilization(39). Therefore, the homeostasis
515 of the PPARγ/UCP2 axis is critical in maintaining normal placental function.
516
517 It is interesting to note that Rnd3 facilitates the protein accumulation of PPARγ
518 without causing the change of PPARγ mRNA transcripts. Therefore,
519 immunoprecipitation was performed to investigate the underlying mechanism, and the

direct interaction of protein molecules of RND3 and PPARγ was observed. Meanwhile, the co-localization of the two proteins was visualized in nuclei and cytoplasm (Fig 6G). Given that the dynamics of PPARγ depends on ligand-induced transcriptional activation and ubiquitin-proteasome dependent degradation, it is reasonable that Rnd3 may stabilize PPARγ in a post-translational manner.

The present study has several limitations. First, even though we have used two cell models, including PE primary cell and the transformed BeWo cell line, to mimic the Rnd3 downregulation in PE patients' placentas. It is not precisely clear whether Rnd3 deficiency could cause PE *in vivo*. Future studies using the *Rnd3* gene knockout animal model will provide stronger supports for the role of Rnd3 in PE pathogenesis. Second, even though we have proved the direct interaction of RND3 and PPARγ protein molecules; however, the more precise post-translational regulation mechanism also needs further investigation.

Conclusions

We identified here the downregulation of Rnd3 in placental trophoblasts in patients with PE and proved that Rnd3 deficiency could cause mitochondrial defects and oxidative stress in trophoblasts. Supply of Rnd3 in PE primary trophoblasts attenuated mitochondrial dysfunction and oxidative stress. The possible underlying mechanism is that Rnd3 interacts with PPARγ and stabilizes PPARγ protein, causing stimulation of PPARγ/UCP2 cascade. In conclusion, our study indicates the novel role of Rnd3, providing new insights into PE pathogenesis.

Disclosure of interests

None.

Contribution to authorship

X.Y. designed the experiments; L.H., Y.M. and X.Y. conducted most experiments; L.C. collected data in Fig. 9; Y.S., X.C., F.S., L.X., J.C., Y.L., C.Y. and X.Y. analyzed the data; X.Y. wrote the manuscript; J.C., M.Z., Z.W. and X.Y. revised the manuscript. All

authors contributed to the final manuscript.

Funding

This study was supported by the following funding sources: the Major Science and Technology Program of Hainan Province (ZDKJ2017007), the National Natural Science Foundation of China (81771609, 81601317, 81960283, and 81971415), the Natural Science Foundation of Guangdong Province (2017A030313584, 2019A1515010290 and 2019A1515010019), the Special Fund for Cooperative Innovation and Platform Environment Construction (2015B050501006), the Outstanding Youth Development Scheme of Nanfang Hospital Southern Medical University (2018J010).

References

1. Rana, S., Lemoine, E., Granger, J. P., and Karumanchi, S. A. (2019) Preeclampsia: Pathophysiology, Challenges, and Perspectives. *Circ Res* **124**, 1094-1112
2. Steegers, E. A., von Dadelszen, P., Duvekot, J. J., and Pijnenborg, R. (2010) Pre-eclampsia. *Lancet* **376**, 631-644
3. Hladunewich, M., Karumanchi, S. A., and Lafayette, R. (2007) Pathophysiology of the clinical manifestations of preeclampsia. *Clin J Am Soc Nephrol* **2**, 543-549
4. Birben, E., Sahiner, U. M., Sackesen, C., Erzurum, S., and Kalayci, O. (2012) Oxidative stress and antioxidant defense. *World Allergy Organ J* **5**, 9-19
5. San Juan-Reyes, S., Gomez-Olivan, L. M., Islas-Flores, H., and Dublan-Garcia, O. (2020) Oxidative stress in pregnancy complicated by preeclampsia. *Arch Biochem Biophys* **681**, 108255
6. Myatt, L. (2010) Review: Reactive oxygen and nitrogen species and functional adaptation of the placenta. *Placenta* **31 Suppl**, S66-69
7. Sanchez-Aranguren, L. C., Prada, C. E., Riano-Medina, C. E., and Lopez, M. (2014) Endothelial dysfunction and preeclampsia: role of oxidative stress. *Front Physiol* **5**, 372
8. Wang, Y., and Walsh, S. W. (1998) Placental mitochondria as a source of oxidative stress in pre-eclampsia. *Placenta* **19**, 581-586
9. D'Souza, V., Rani, A., Patil, V., Pisal, H., Randhir, K., Mehendale, S., Wagh, G., Gupte, S., and Joshi, S. (2016) Increased oxidative stress from early pregnancy in women who develop preeclampsia. *Clin Exp Hypertens* **38**, 225-232
10. Vishnyakova, P. A., Volodina, M. A., Tarasova, N. V., Marey, M. V., Tsvirkun, D. V., Vavina, O. V., Khodzhaeva, Z. S., Kan, N. E., Menon, R., Vysokikh, M. Y., and Sukhikh, G. T. (2016)

587 Mitochondrial role in adaptive response to stress conditions in preeclampsia. *Sci Rep* **6**,
588 32410
589 11. Salgado, S. S., and Salgado, M. K. R. (2011) Structural changes in pre-eclamptic and
590 eclamptic placentas--an ultrastructural study. *J Coll Physicians Surg Pak* **21**, 482-486
591 12. Janani, C., and Ranjitha Kumari, B. D. (2015) PPAR gamma gene--a review. *Diabetes*
592 *Metab Syndr* **9**, 46-50
593 13. Corona, J. C., and Duchen, M. R. (2016) PPARgamma as a therapeutic target to rescue
594 mitochondrial function in neurological disease. *Free Radic Biol Med* **100**, 153-163
595 14. Waite, L. L., Louie, R. E., and Taylor, R. N. (2005) Circulating activators of peroxisome
596 proliferator-activated receptors are reduced in preeclamptic pregnancy. *J Clin Endocrinol*
597 *Metab* **90**, 620-626
598 15. Barak, Y., Nelson, M. C., Ong, E. S., Jones, Y. Z., Ruiz-Lozano, P., Chien, K. R., Koder, A.,
599 and Evans, R. M. (1999) PPAR gamma is required for placental, cardiac, and adipose
600 tissue development. *Mol Cell* **4**, 585-595
601 16. Barak, Y., Liao, D., He, W., Ong, E. S., Nelson, M. C., Olefsky, J. M., Boland, R., and Evans, R.
602 M. (2002) Effects of peroxisome proliferator-activated receptor delta on placentation,
603 adiposity, and colorectal cancer. *Proc Natl Acad Sci U S A* **99**, 303-308
604 17. Schaiff, W. T., Carlson, M. G., Smith, S. D., Levy, R., Nelson, D. M., and Sadovsky, Y. (2000)
605 Peroxisome proliferator-activated receptor-gamma modulates differentiation of human
606 trophoblast in a ligand-specific manner. *J Clin Endocrinol Metab* **85**, 3874-3881
607 18. Waite, L. L., Person, E. C., Zhou, Y., Lim, K. H., Scanlan, T. S., and Taylor, R. N. (2000)
608 Placental peroxisome proliferator-activated receptor-gamma is up-regulated by
609 pregnancy serum. *J Clin Endocrinol Metab* **85**, 3808-3814
610 19. McCarthy, F. P., Drewlo, S., Kingdom, J., Johns, E. J., Walsh, S. K., and Kenny, L. C. (2011)
611 Peroxisome proliferator-activated receptor-gamma as a potential therapeutic target in
612 the treatment of preeclampsia. *Hypertension* **58**, 280-286
613 20. Liu, B., Lin, X., Yang, X., Dong, H., Yue, X., Andrade, K. C., Guo, Z., Yang, J., Wu, L., Zhu, X.,
614 Zhang, S., Tian, D., Wang, J., Cai, Q., Chen, Q., Mao, S., Chen, Q., and Chang, J. (2015)
615 Downregulation of RND3/RhoE in glioblastoma patients promotes tumorigenesis
616 through augmentation of notch transcriptional complex activity. *Cancer Med* **4**,
617 1404-1416
618 21. Yue, X., Yang, X., Lin, X., Yang, T., Yi, X., Dai, Y., Guo, J., Li, T., Shi, J., Wei, L., Fan, G. C.,
619 Chen, C., and Chang, J. (2014) Rnd3 haploinsufficient mice are predisposed to
620 hemodynamic stress and develop apoptotic cardiomyopathy with heart failure. *Cell*
621 *Death Dis* **5**, e1284
622 22. Yue, X., Lin, X., Yang, T., Yang, X., Yi, X., Jiang, X., Li, X., Li, T., Guo, J., Dai, Y., Shi, J., Wei, L.,
623 Youker, K. A., Torre-Amione, G., Yu, Y., Andrade, K. C., and Chang, J. (2016) Rnd3/RhoE
624 Modulates Hypoxia-Inducible Factor 1alpha/Vascular Endothelial Growth Factor
625 Signaling by Stabilizing Hypoxia-Inducible Factor 1alpha and Regulates Responsive
626 Cardiac Angiogenesis. *Hypertension* **67**, 597-605
627 23. Yang, X., Wang, T., Lin, X., Yue, X., Wang, Q., Wang, G., Fu, Q., Ai, X., Chiang, D. Y., Miyake,
628 C. Y., Wehrens, X. H. T., and Chang, J. (2015) Genetic deletion of Rnd3/RhoE results in
629 mouse heart calcium leakage through upregulation of protein kinase A signaling. *Circ*
630 *Res* **116**, e1-e10

631 24. Dai, Y., Song, J., Li, W., Yang, T., Yue, X., Lin, X., Yang, X., Luo, W., Guo, J., Wang, X., Lai, S.,
632 Andrade, K. C., and Chang, J. (2019) RhoE Fine-Tunes Inflammatory Response in
633 Myocardial Infarction. *Circulation* **139**, 1185-1198
634 25. Lin, X., Liu, B., Yang, X., Yue, X., Diao, L., Wang, J., and Chang, J. (2013) Genetic deletion of
635 Rnd3 results in aqueductal stenosis leading to hydrocephalus through up-regulation of
636 Notch signaling. *Proc Natl Acad Sci U S A* **110**, 8236-8241
637 26. Moses, E., Johnson, M., East, C., Dyer, T., Roten, L., Proffitt, J., Fenstad, M.,
638 Aalto-Viljakainen, T., Makikallio, K., Heinonen, S., Kajantie, E., Kere, J., Laivuori, H.,
639 Austgulen, R., Blangero, J., and Brennecke, S. (2012) OS077. The chromosome 2q22
640 preeclampsia susceptibility locus reveals shared novel risk factors for CVD. *Pregnancy*
641 *Hypertens* **2**, 219-220
642 27. Xu, Y., Wu, D., Liu, J., Huang, S., Zuo, Q., Xia, X., Jiang, Y., Wang, S., Chen, Y., Wang, T.,
643 and Sun, L. (2018) Downregulated lncRNA HOXA11-AS Affects Trophoblast Cell
644 Proliferation and Migration by Regulating RND3 and HOXA7 Expression in PE. *Mol Ther*
645 *Nucleic Acids* **12**, 195-206
646 28. Xu, Y., Ge, Z., Zhang, E., Zuo, Q., Huang, S., Yang, N., Wu, D., Zhang, Y., Chen, Y., Xu, H.,
647 Huang, H., Jiang, Z., and Sun, L. (2017) The lncRNA TUG1 modulates proliferation in
648 trophoblast cells via epigenetic suppression of RND3. *Cell Death Dis* **8**, e3104
649 29. Fang, Y. N., Huang, Z. L., Li, H., Tan, W. B., Zhang, Q. G., Wang, L., and Wu, J. L. (2018)
650 Highly expressed miR-182-5p can promote preeclampsia progression by degrading
651 RND3 and inhibiting HTR-8/SVneo cell invasion. *Eur Rev Med Pharmacol Sci* **22**,
652 6583-6590
653 30. Yue, X., Sun, Y., Zhong, M., Ma, Y., Wei, Y., Sun, F., Xiao, L., Liu, M., Chen, J., Lai, Y., Yan, C.,
654 Huang, L., and Yu, Y. (2018) Decreased expression of fibroblast growth factor 13 in
655 early-onset preeclampsia is associated with the increased trophoblast permeability.
656 *Placenta* **62**, 43-49
657 31. Medvedev, A. V., Snedden, S. K., Raimbault, S., Ricquier, D., and Collins, S. (2001)
658 Transcriptional regulation of the mouse uncoupling protein-2 gene. Double E-box motif
659 is required for peroxisome proliferator-activated receptor-gamma-dependent activation.
660 *J Biol Chem* **276**, 10817-10823
661 32. Torbergsen, T., Oian, P., Mathiesen, E., and Borud, O. (1989) Pre-eclampsia--a
662 mitochondrial disease? *Acta Obstet Gynecol Scand* **68**, 145-148
663 33. Shi, Z., Long, W., Zhao, C., Guo, X., Shen, R., and Ding, H. (2013) Comparative proteomics
664 analysis suggests that placental mitochondria are involved in the development of
665 pre-eclampsia. *PLoS One* **8**, e64351
666 34. Collett, G. P., Goh, X. F., Linton, E. A., Redman, C. W. G., Sargent, I. L. (2012) RhoE is
667 regulated by cyclic AMP and promotes fusion of human BeWo choriocarcinoma cells.
668 *PLoS One* **7**, e30453
669 35. Saso, J., Shields, S., Zuo, Y., Chakraborty, C. (2012) Role of Rho GTPases in human
670 trophoblast migration induced by IGFBP1. *Biol Reprod* **86**,1-9.
671 36. Jie, W., Andrade, K. C., Lin, X., Yang, X., Yue, X., Chang, J. (2015) Pathophysiological
672 Functions of Rnd3/RhoE. *Compr Physiol* **6**, 169-186.
673 37. Cadenas, S. (2018) Mitochondrial uncoupling, ROS generation and cardioprotection.
674 *Biochim Biophys Acta Bioenerg* **1859**, 940-950

38. Kohan-Ghadr, H. R., Kilburn, B. A., Kadam, L., Johnson, E., Kolb, B. L., Rodriguez-Kovacs, J., Hertz, M., Armant, D. R., and Drewlo, S. (2019) Rosiglitazone augments antioxidant response in the human trophoblast and prevents apoptosisdagger. *Biol Reprod* **100**, 479-494

39. Yiallourides, M., Sebert, S. P., Wilson, V., Sharkey, D., Rhind, S. M., Symonds, M. E., and Budge, H. (2009) The differential effects of the timing of maternal nutrient restriction in the ovine placenta on glucocorticoid sensitivity, uncoupling protein 2, peroxisome proliferator-activated receptor-gamma and cell proliferation. *Reproduction* **138**, 601-608

Table 1. Clinical characteristics of the PE group and of the healthy control group. Clinical data of blood pressure, BMI and proteinuria was collected at the time of PE diagnosis.

Figure 1. The expression of Rnd3 is downregulated in human placentae with PE. (**A**) Representative RND3 protein expression by Western blot analysis. Densitometry of bands was performed by Image J. (**B**) Relative levels of *Rnd3* mRNA from 34 human healthy placentae and 24 human placentae with PE.

Figure 2. Decreased Rnd3 expression levels are associated with severe oxidative stress and apoptosis in PE patient derived-human primary trophoblasts. (**A**) Severe oxidative stress was observed in human placental tissue sections from PE patients by DHE staining. The nuclei were visualized by blue DAPI staining. Scale bar represents 200 μm. (**B**) Isolated human primary trophoblast cells (PTBs) were identified by the cell surface marker CK7 shown in red and the nuclei were visualized by DAPI. The purity of primary trophoblasts was calculated by the ratio of CK7-positive cells over nuclei. The scale bar represents 200 μm. (**C**) RND3 protein expression in PTBs was labeled by immunostaining. Decreased Rnd3 expression along with increased ROS levels were observed in the PTBs from PE patients. The scale bar represents 5 μm. (**D**) Elevated ROS levels and severe apoptosis were observed in the PE PTBs compared with those of the PTBs from healthy control subjects. ROS was labeled by DHE staining shown in red. The arrows point at the TUNEL-positive cells (green), which overlapped with nuclear counter-staining (blue). The scale bar represents 40 μm.

Figure 3. Abnormal mitochondria were observed in the human placental trophoblasts with PE. (**A**) Placental tissues from PE patients and healthy control subjects were analyzed by transmission electron microscopy and viewed at a low magnification (upper panel) and a high magnification (lower panel), respectively. The arrows point at the damaged mitochondria with loss of cristae (LOC). The scale bars represent 1 μm and 500 nm, respectively. (**B**) Mitochondrial membrane potentials

719 were shown by the JC1 staining of the primary trophoblast cells isolated from PE
720 patients and healthy control subjects with or without hypoxic cell culture. JC1 is a cell
721 permeable dye that accumulates in mitochondria and yields green fluorescence.
722 Driven by high mitochondrial membrane potential, JC1 is able to enter the
723 mitochondrial inner membrane and yield red fluorescence. The ratios of the red/green
724 fluorescence intensities were quantified by the image J software. The numbers in the
725 columns represent the numbers of cells in each group. C-PTBs indicates
726 control-primary trophoblasts, and P-PTBs indicates PE-primary trophoblasts.
727
728 **Figure 4. Rnd3 represses the hypoxia-induced ROS generation and apoptosis in**
729 **trophoblastic BeWo cells.** (**A**) Challenged with hypoxic condition, GFP-Rnd3
730 overexpressing BeWo cells exhibited reduced ROS levels. ROS was labeled by DHE
731 staining shown in red. The arrows point at the GFP-Rnd3 expressing cells. The scale
732 bar represents 80 μm. (**B**) A decrease in 8-isoprostane levels was detected in the cell
733 lysates of myc-Rnd3 overexpressing BeWo cells, compared with those noted in the
734 myc control group. The experiments were repeated 3 times. (**C**) The comparison of
735 the TUNEL staining in myc and myc-Rnd3 overexpressing BeWo cells following 16 h
736 of hypoxic cell culture. The arrows indicate TUNEL-positive cells (green)
737 overlapping with nuclear counter-staining. The scale bar represents 200 μm. (**D**)
738 Quantification of TUNEL-positive cells. The experiments were repeated 3 times.
739
740 **Figure 5. Rnd3 deficiency results in mitochondrial dysfunction.** (**A**) By
741 transmission electron microscope analysis, mitochondrial damage was observed in
742 siRnd3 transiently transfected BeWo cells. The arrow heads indicate the loss of cristae
743 (LOC) in the damaged mitochondria. The images of a series of magnifications are
744 displayed. (**B**) The depolarized mitochondrial membrane potential was detected in
745 siRnd3 transfected BeWo cells compared with that noted in the siCtrl group. The
746 mitochondrial membrane potential was quantified by the ratios of red/green
747 fluorescence intensities of mitochondria-specific JC1 dye. The scale bar represents 80
748 μm. (**C**) The Oxygen consumption rate (OCR) of treated BeWo cells was measured
749 prior to and following the injections of oligomycin, FCCP, rotenone and antimycin A
750 (Rot/AA), respectively. Increased proton leak was detected in the siRnd3 group. (**D**)
751 Reduced coupler efficiency was detected in siRnd3 transfected BeWo cells compared
752 with that noted in the siCtrl group as determined by mitochondrial OCR determination.
753 The numbers in the columns represent the number of cells in each group.
754
755 **Figure 6. RND3 protein interacts with PPARγ and promotes the PPARγ-UCP2**
756 **cascade.** (**A**) Increased expression levels of UCP2 and PPARγ were observed
757 following Rnd3 overexpression. (**B**) Knockdown of Rnd3 results in lower UCP2 and
758 PPARγ protein expression levels. (**C**) Q-PCR analysis indicated that *UCP2* mRNA
759 levels were increased in myc-Rnd3 expressed cells, whereas they were reduced in
760 Rnd3 deficient cells. (**D**) Nuclear protein levels of RND3 and PPARγ were increased
761 in the myc-Rnd3 overexpressed cells and were decreased in the Rnd3 deficient cells.

762 (**E**) Rnd3 regulated PPARγ transcriptional activity as demonstrated by luciferase
763 assays. (**F**) Myc-RND3 physically interacted with flag-PPARγ *in vivo* as determined
764 by coimmunoprecipitation. (**G**) Immunofluorescence staining indicated the
765 co-localization of PPARγ and RND3 proteins. Knockdown of Rnd3 reduced the
766 nuclear accumulation of the PPARγ protein. The scale bar represents 100 μm.
767
768 **Figure 7. Rnd3 deficiency-mediated oxidative stress and mitochondrial**
769 **dysfunction are attenuated by PPARγ overexpression.** (**A**) JC1 staining was
770 performed in BeWo cells among the three following groups: siCtrl, siRnd3 and
771 siRnd3 plus flag-PPARγ. The depolarization of the mitochondrial membrane potential
772 caused by Rnd3 knockdown was attenuated by flag-PPARγ overexpression. The scale
773 bar represents 80 μm. (**B**) The quantification of the ratios of red/green fluorescence
774 intensities. The experiments were repeated 3 times. (**C**) Transmission electron
775 microscope analysis indicates that the Rnd3 deficiency-induced mitochondrial
776 damage was recovered by flag-PPARγ overexpression. The arrow heads display
777 damaged mitochondrial structure in the siRnd3 group. The scale bar represents 0.5 μm.
778 (**D**) DHE staining indicates ROS levels among the three groups. The scale bar
779 represents 100 μm. (**E**) The ROS levels were quantified by the densitometry of DHE
780 staining. The experiments were repeated 3 times. (**F**) 8-isoprostane levels were
781 detected in the cell lysates of the three groups. (**G**) Q-PCR analysis of *UCP2* mRNA
782 levels among the three groups. The experiments were repeated 3 times. (**H**)
783 Immunoblots revealed increased UCP2 protein expression levels in the flag-PPARγ
784 rescue group. (**I**) Mitochondrial respiratory function was measured. The proton leak
785 associated OCR was improved by PPARγ. (**J**) Rnd3 deficiency-mediated defective
786 coupler efficiency was ameliorated by PPARγ.
787
788 **Figure 8. Oxidative stress and mitochondrial dysfunction in PE patient-derived**
789 **PTBs are partially rescued by Rnd3 overexpression. (A**) Human PTBs from PE
790 patient and healthy control subjects were infected with Ad-GFP-hRnd3. Hypoxic cell
791 culture was applied to induce oxidative stress. The arrow heads represent the
792 GFP-Rnd3 expressing PTBs (green fluorescence). The long arrows represent the
793 PTBs with non-GFP-Rnd3. ROS levels were significantly reduced in PE-PTBs
794 following GFP-Rnd3 overexpression as determined by DHE staining. NS indicates
795 non-specific staining. The scale bar represents 25 μm. (**B**) 8-isoprostane level
796 detection in the C-PTBs and P-PTBs following treatment of Ad-GFP or
797 Ad-GFP-Rnd3. (**C**) Ad-GFP-hRnd3 improved *UCP2* mRNA transcripts in the PTBs.
798 (**D**) Rnd3 overexpression rescued PPARγ-UCP2 signaling in PE-PTBs. Mitochondrial
799 dysfunction in PE-PTBs was partially rescued by Ad-GFP-hRnd3, as determined by
800 the increases in proton leak associated OCR (**E**) and respiratory control ratio (**F**).
801 C-PTBs indicates control-primary trophoblasts; P-PTBs, PE-primary trophoblasts.
802
803 **Figure 9. The downregulation of the PPARγ-UCP2 cascade is confirmed in**
804 **human placentae with PE. (A)** Representative protein expression levels of PPARγ
805 and UCP2 as determined by western blot analysis. The levels of the two proteins were

806 downregulated in the placentas with PE. (**B**) Relative mRNA levels of *PPARγ* from 34
807 healthy placentae and 24 placentae with PE. (**C**) Relative mRNA levels of *UCP2* from
808 34 healthy placentae and 24 placentae with PE.
809
810
811
812

Figure 1

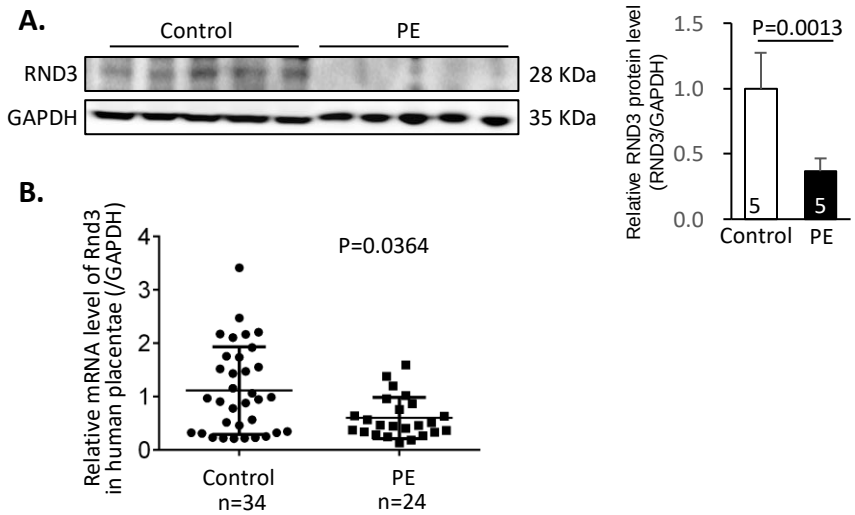
A.
Control
PE
RND3
28 KDa
GAPDH
35 KDa
B.
Relative mRNA level of Rnd3 in human placentae (/GAPDH)
P=0.0364
Control n=34
PE n=24
Relative RND3 protein level (RND3/GAPDH)
P=0.0013
Control
PE

Figure 2

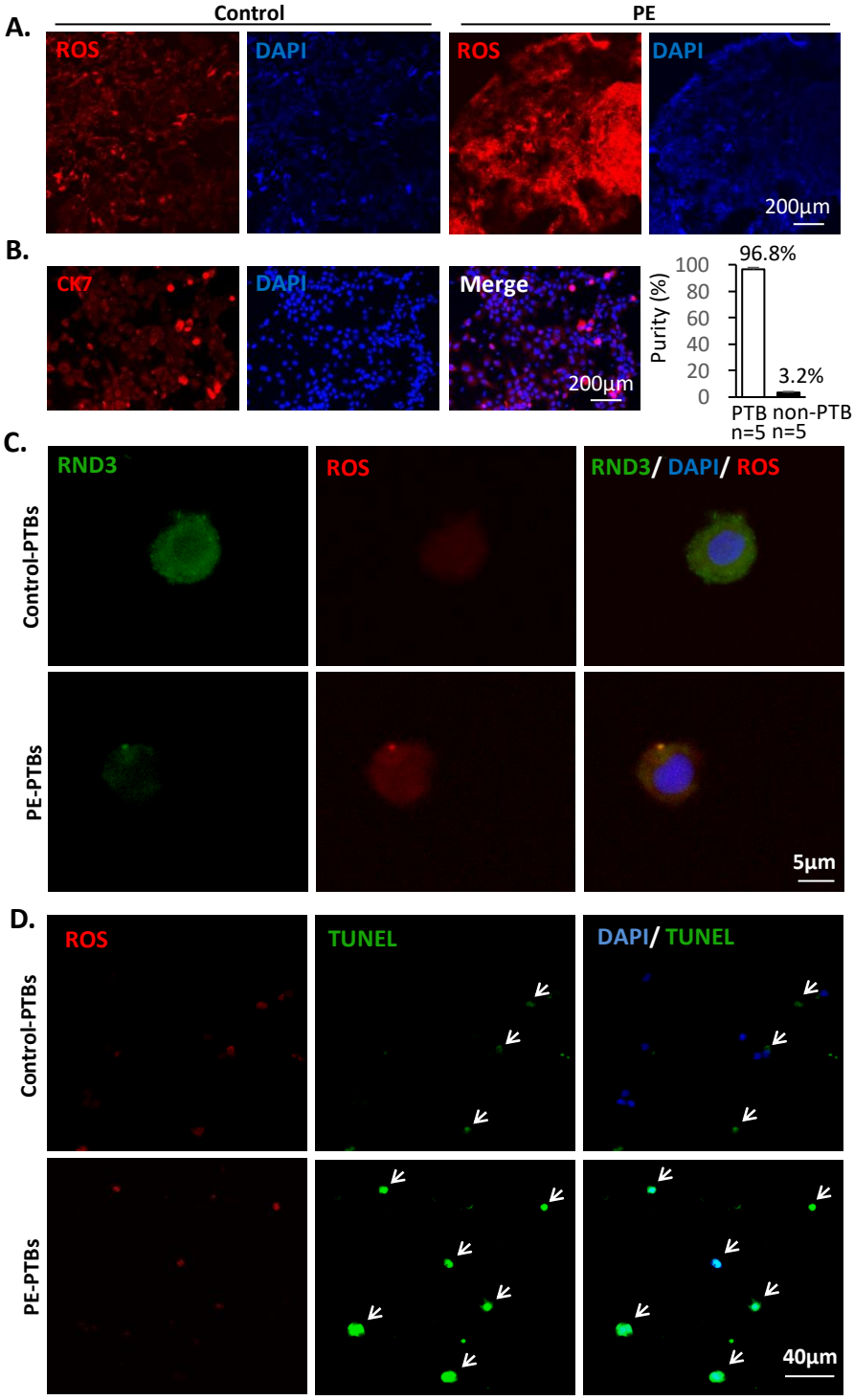
A.
Control
PE
ROS
DAPI
ROS
DAPI
200μm
B.
CK7
DAPI
Merge
200μm
Purity (%)
100
80
60
40
20
0
96.8%
3.2%
PTB n=5
non-PTB n=5
C.
Control-PTBs
PE-PTBs
RND3
ROS
RND3/ DAPI/ ROS
5μm
D.
Control-PTBs
PE-PTBs
ROS
TUNEL
DAPI/ TUNEL
40μm

Figure 3

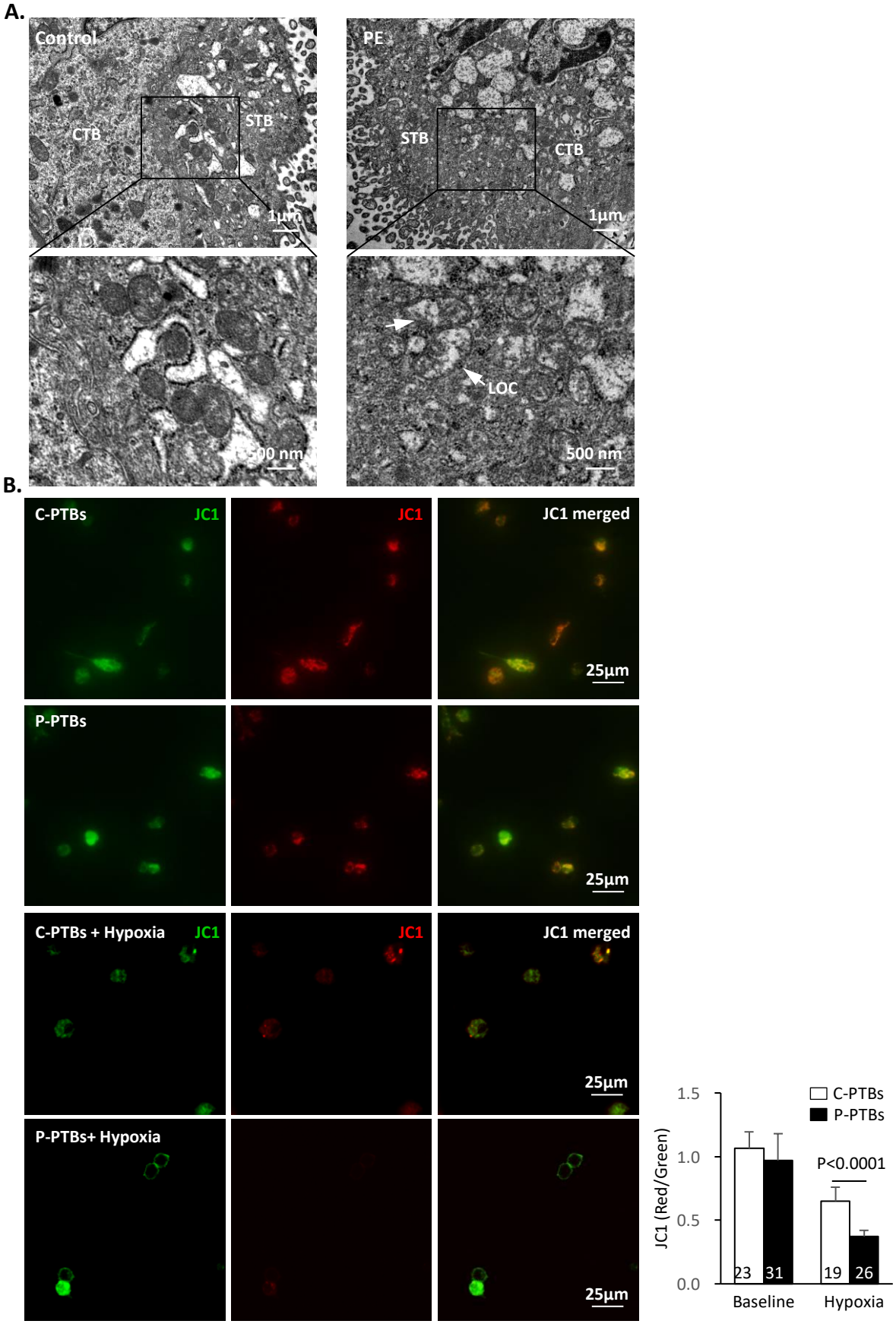
A.
Control
CTB
STB
1µm
500 nm
PE
STB
CTB
1µm
LOC
500 nm
B.
C-PTBs
JC1
JC1
JC1 merged
25µm
P-PTBs
25µm
C-PTBs + Hypoxia
JC1
JC1
JC1 merged
25µm
P-PTBs+ Hypoxia
25µm
C-PTBs
P-PTBs
JC1 (Red/Green)
1.5
1.0
0.5
0.0
P<0.0001
23
31
19
26
Baseline
Hypoxia

Figure 4

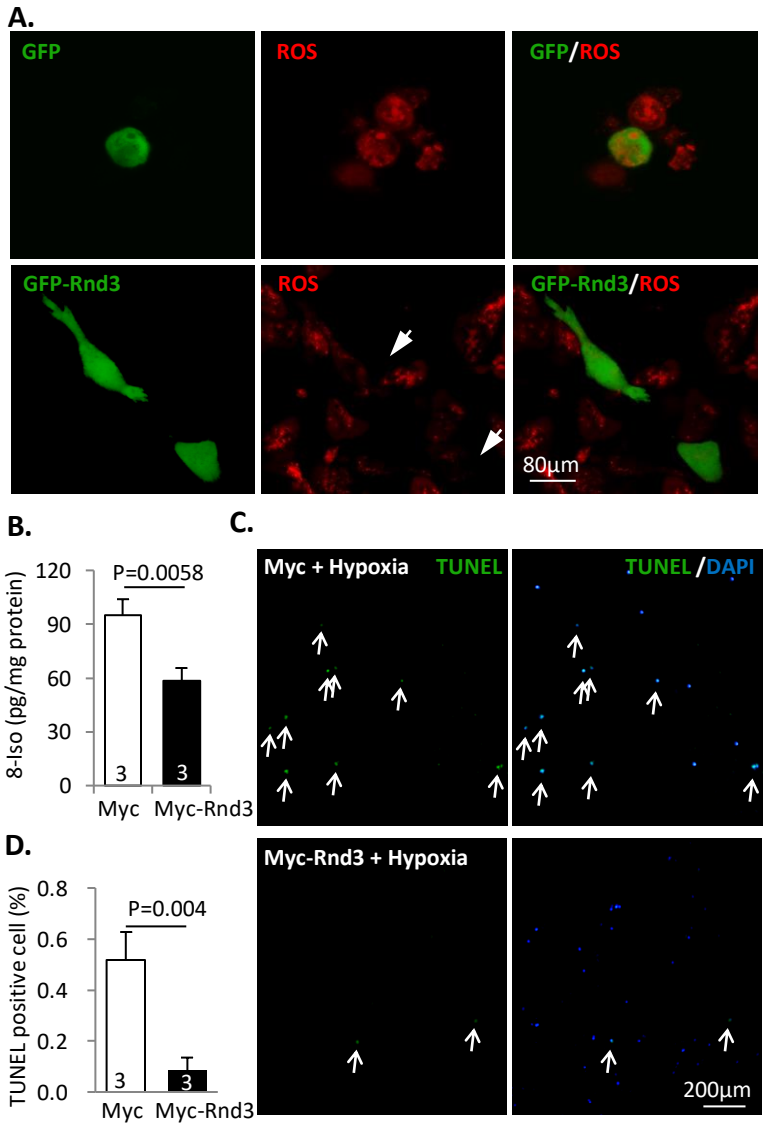
A.
GFP
ROS
GFP/ROS
GFP-Rnd3
ROS
GFP-Rnd3/ROS
80μm
B.
8-Iso (pg/mg protein)
120
90
60
30
0
P=0.0058
3
3
Myc
Myc-Rnd3
C.
Myc + Hypoxia
TUNEL
TUNEL /DAPI
Myc-Rnd3 + Hypoxia
200μm
D.
TUNEL positive cell (%)
0.8
0.6
0.4
0.2
0.0
P=0.004
3
3
Myc
Myc-Rnd3

Figure 5

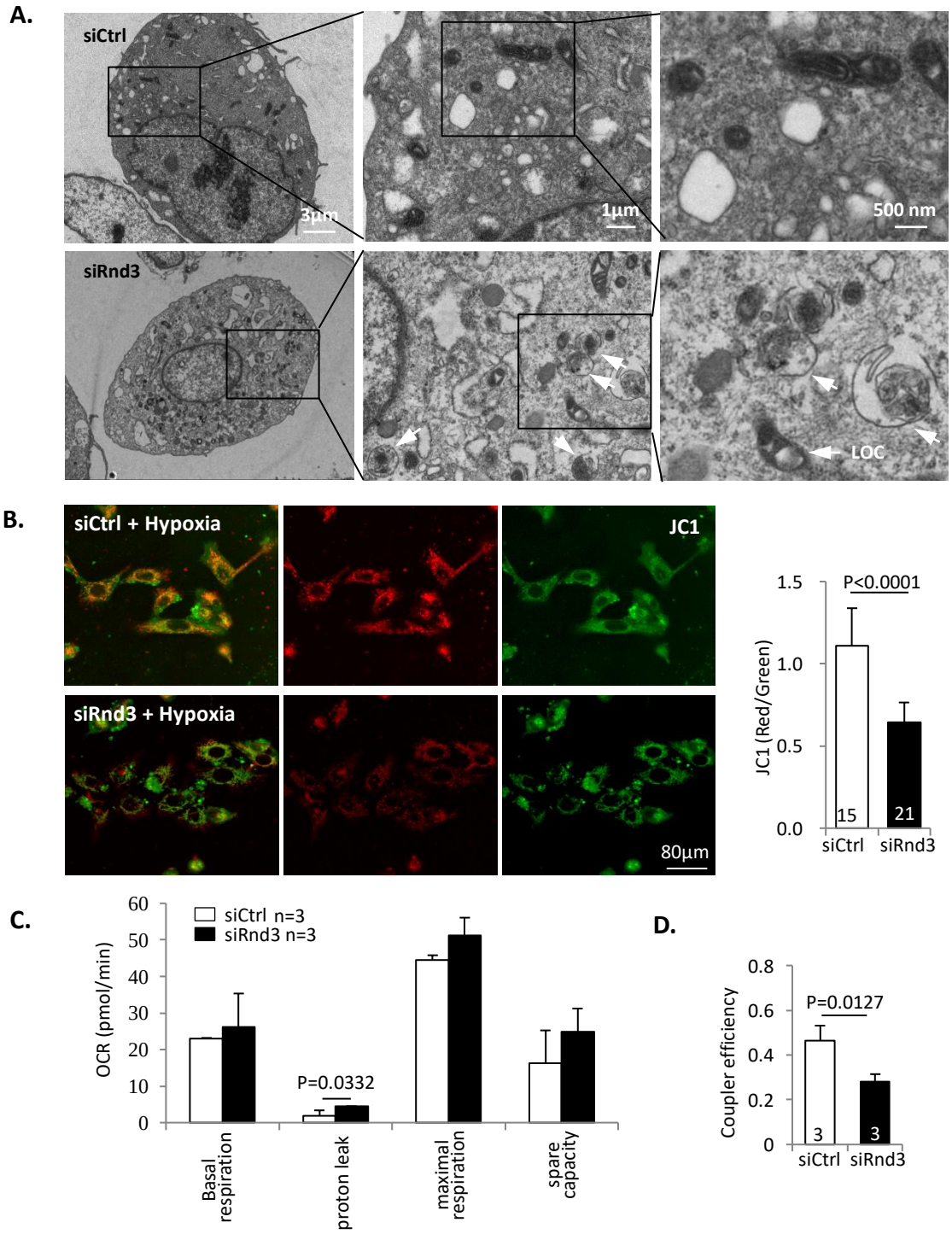
A.
siCtrl
3µm
1µm
500 nm
siRnd3
LOC
B.
siCtrl + Hypoxia
JC1
siRnd3 + Hypoxia
80µm
P<0.0001
JC1 (Red/Green)
1.5
1.0
0.5
0.0
15
21
siCtrl
siRnd3
C.
siCtrl n=3
siRnd3 n=3
OCR (pmol/min)
60
50
40
30
20
10
0
P=0.0332
Basal respiration
proton leak
maximal respiration
spare capacity
D.
P=0.0127
Coupler efficiency
0.8
0.6
0.4
0.2
0
3
3
siCtrl
siRnd3

Figure 6

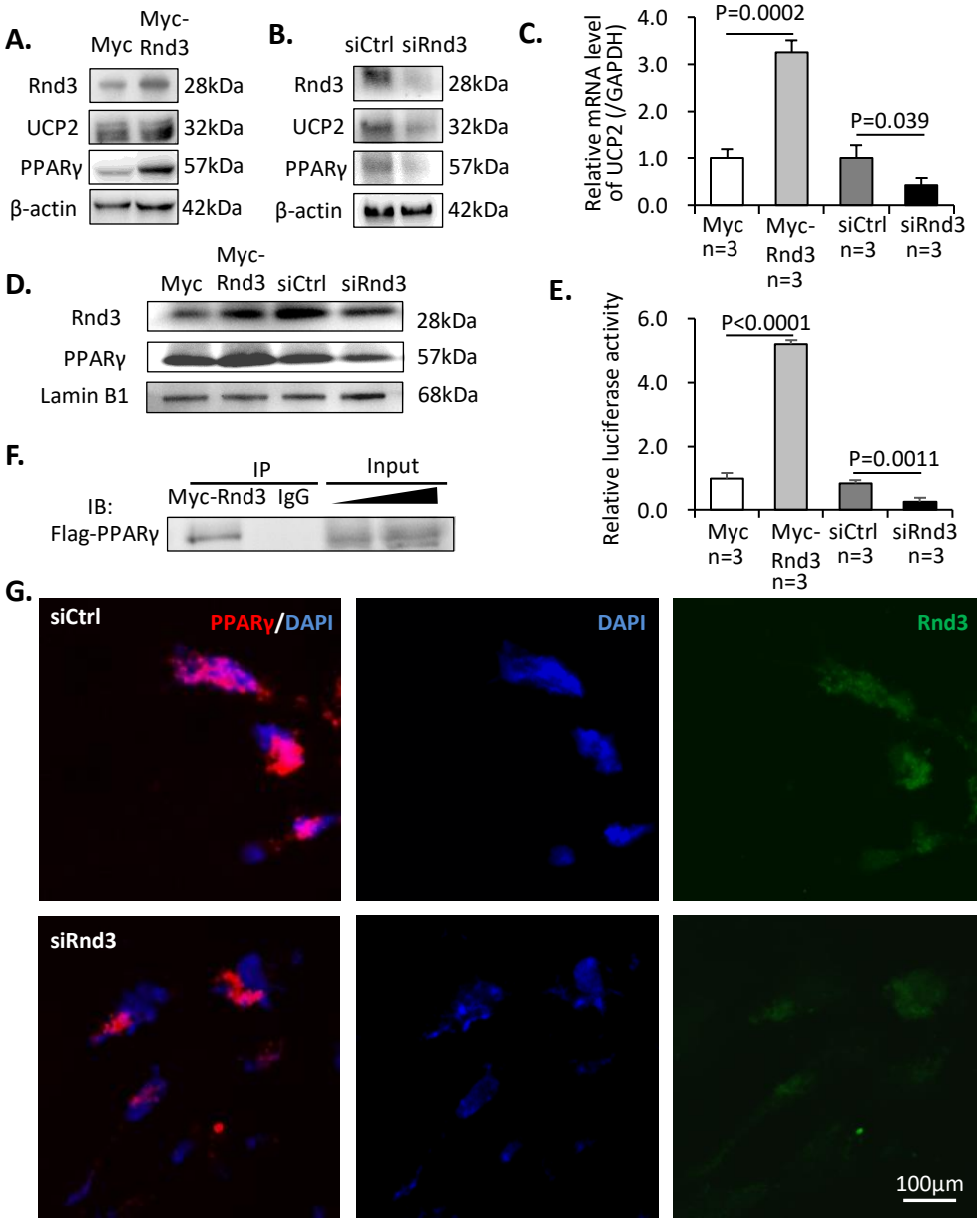
A.
Myc
Myc-Rnd3
Rnd3
UCP2
PPARγ
β-actin
28kDa
32kDa
57kDa
42kDa
B.
siCtrl
siRnd3
Rnd3
UCP2
PPARγ
β-actin
28kDa
32kDa
57kDa
42kDa
C.
Relative mRNA level of UCP2 (/GAPDH)
4.0
3.0
2.0
1.0
0.0
P=0.0002
P=0.039
Myc n=3
Myc-Rnd3 n=3
siCtrl n=3
siRnd3 n=3
D.
Myc
Myc-Rnd3
siCtrl
siRnd3
Rnd3
PPARγ
Lamin B1
28kDa
57kDa
68kDa
E.
Relative luciferase activity
6.0
4.0
2.0
0.0
P<0.0001
P=0.0011
Myc n=3
Myc-Rnd3 n=3
siCtrl n=3
siRnd3 n=3
F.
IP
Input
IB:
Myc-Rnd3
IgG
Flag-PPARγ
G.
siCtrl
PPARγ/DAPI
DAPI
Rnd3
siRnd3
100μm

Figure 7

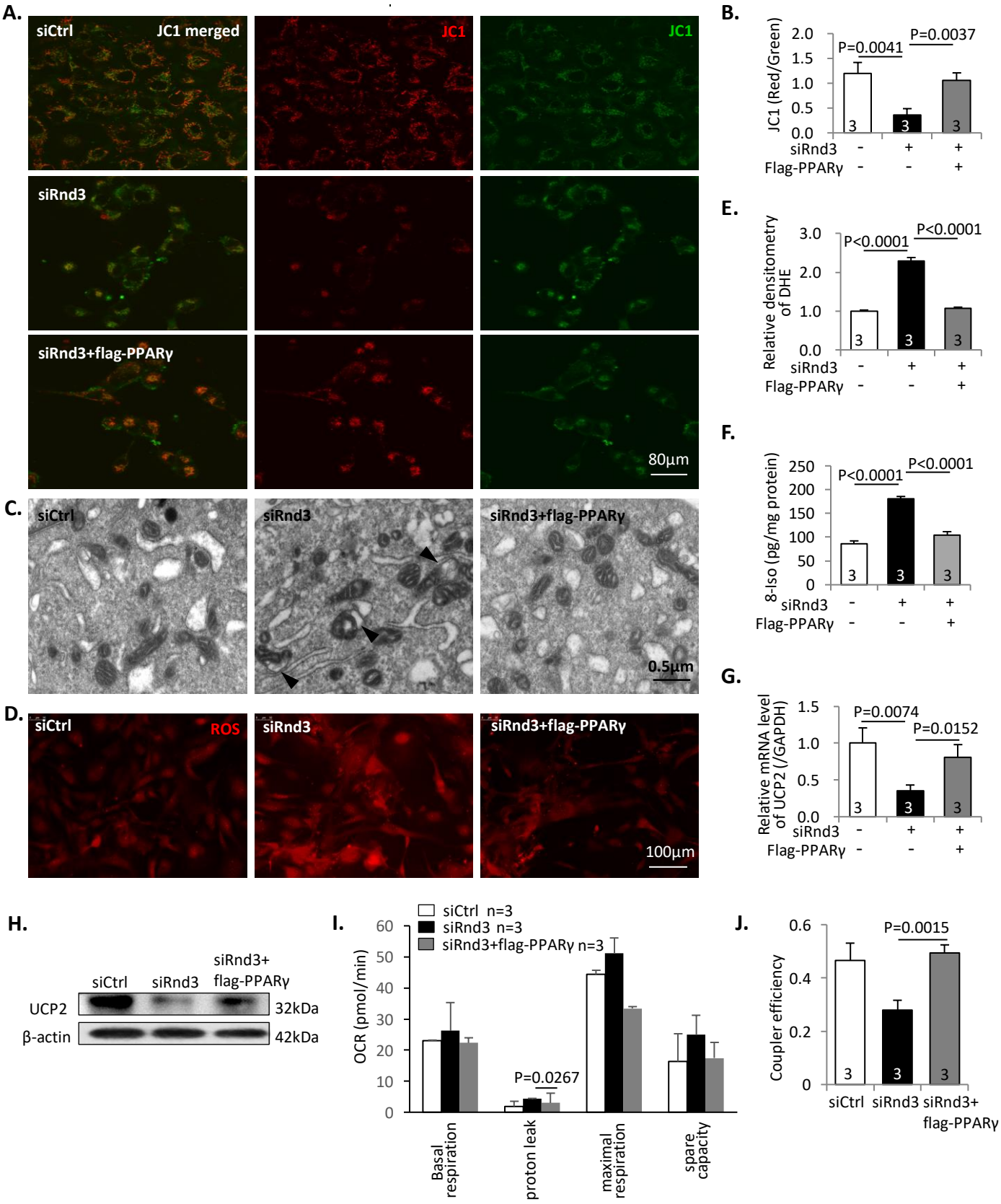
A.
siCtrl
JC1 merged
JC1
JC1
siRnd3
siRnd3+flag-PPARγ
80μm
B.
JC1 (Red/Green)
P=0.0041
P=0.0037
siRnd3
Flag-PPARγ
C.
siCtrl
siRnd3
siRnd3+flag-PPARγ
0.5μm
D.
siCtrl
ROS
siRnd3
siRnd3+flag-PPARγ
100μm
E.
Relative densitometry of DHE
P<0.0001
P<0.0001
F.
8-Iso (pg/mg protein)
P<0.0001
P<0.0001
G.
Relative mRNA level of UCP2 (/GAPDH)
P=0.0074
P=0.0152
H.
siCtrl
siRnd3
siRnd3+ flag-PPARγ
UCP2
β-actin
32kDa
42kDa
I.
siCtrl n=3
siRnd3 n=3
siRnd3+flag-PPARγ n=3
OCR (pmol/min)
P=0.0267
Basal respiration
proton leak
maximal respiration
spare capacity
J.
Coupler efficiency
P=0.0015
siCtrl
siRnd3
siRnd3+ flag-PPARγ

Figure 8

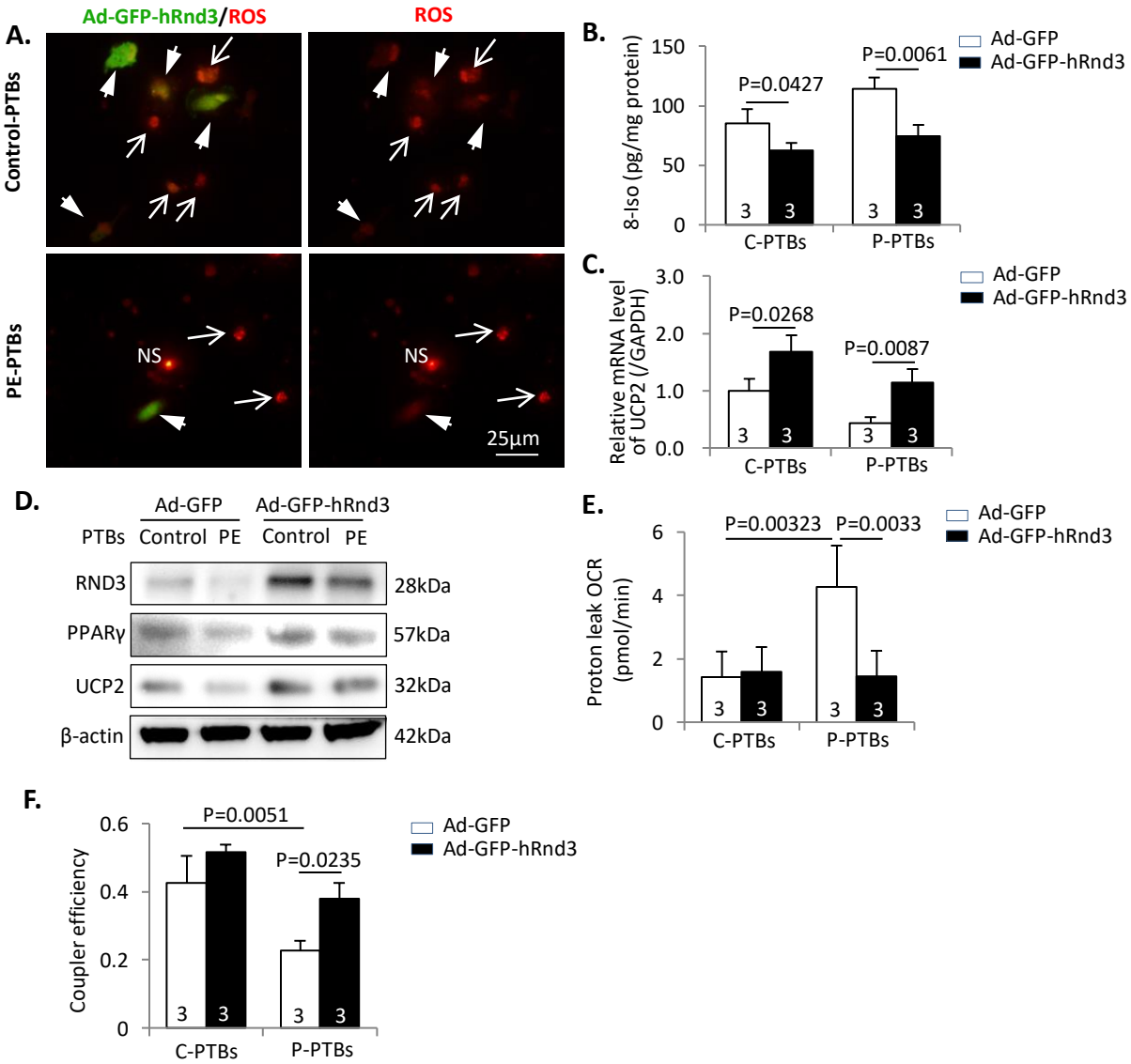
A.
Ad-GFP-hRnd3/ROS
ROS
Control-PTBs
PE-PTBs
NS
NS
25µm
B.
8-Iso (pg/mg protein)
150
100
50
0
P=0.0427
P=0.0061
Ad-GFP
Ad-GFP-hRnd3
3
3
3
3
C-PTBs
P-PTBs
C.
Relative mRNA level of UCP2 (/GAPDH)
3.0
2.0
1.0
0.0
P=0.0268
P=0.0087
Ad-GFP
Ad-GFP-hRnd3
C-PTBs
P-PTBs
D.
Ad-GFP
Ad-GFP-hRnd3
PTBs
Control
PE
Control
PE
RND3
28kDa
PPARγ
57kDa
UCP2
32kDa
β-actin
42kDa
E.
Proton leak OCR (pmol/min)
6
4
2
0
P=0.00323
P=0.0033
Ad-GFP
Ad-GFP-hRnd3
C-PTBs
P-PTBs
F.
Coupler efficiency
0.6
0.4
0.2
0
P=0.0051
P=0.0235
Ad-GFP
Ad-GFP-hRnd3
C-PTBs
P-PTBs

Figure 9

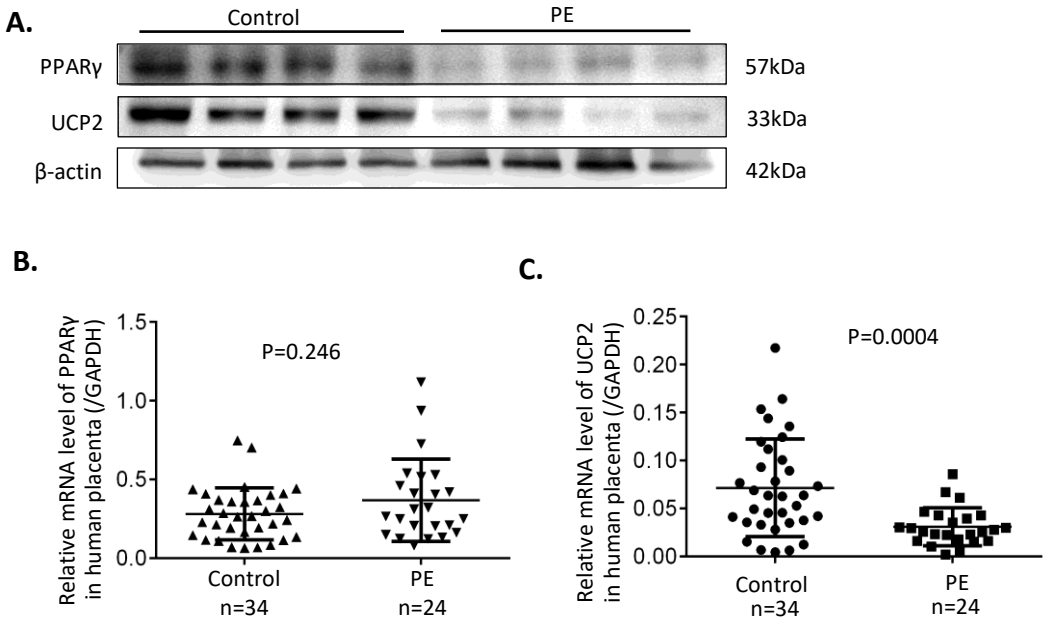
A.
Control
PE
PPARγ
UCP2
β-actin
57kDa
33kDa
42kDa
B.
Relative mRNA level of PPARγ in human placenta (/GAPDH)
1.5
1.0
0.5
0.0
P=0.246
Control n=34
PE n=24
C.
Relative mRNA level of UCP2 in human placenta (/GAPDH)
0.25
0.20
0.15
0.10
0.05
0.00
P=0.0004
Control n=34
PE n=24

Figure S1

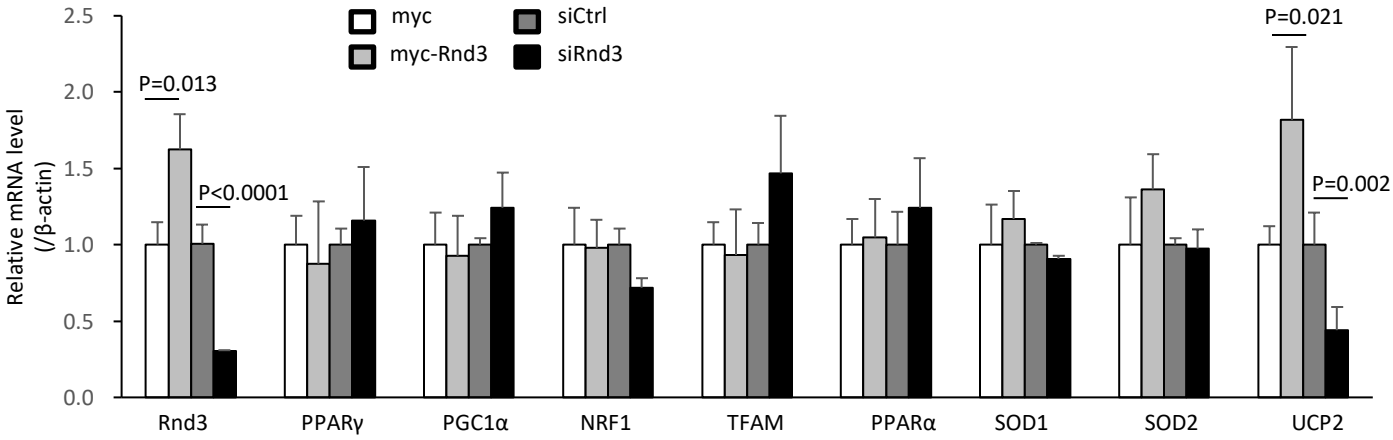

Figure S1. Relative mRNA expression levels of the mitochondrion-related genes in BeWo cells. Rnd3 promoted *UCP2* mRNA level. Manipulation of Rnd3 expression resulted in no change in the mRNA levels of *PPARγ*, *PGC1α*, *NRF1*, *TFAM*, *PPARα*, *SOD1* and *SOD2*.

Figure S2

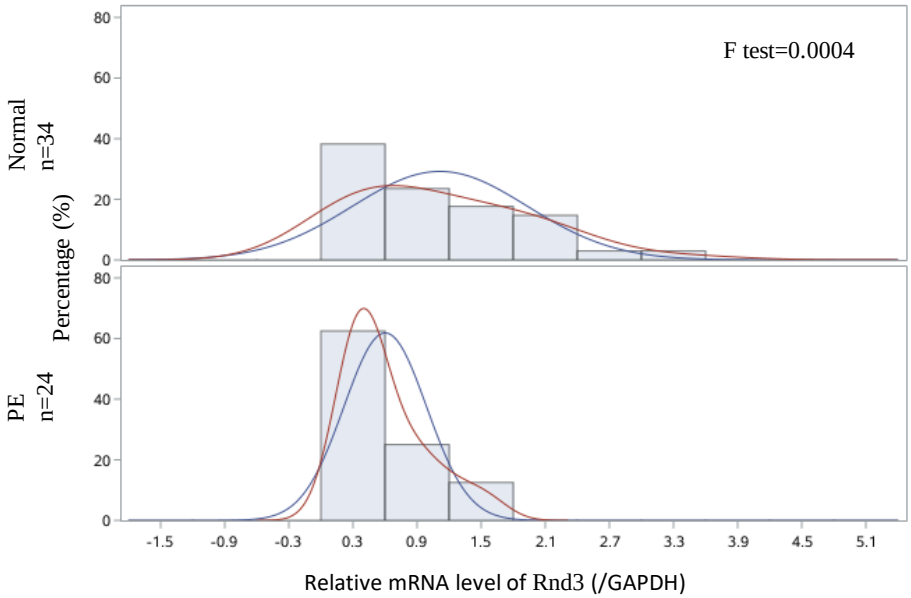

Figure S2. Tests of homogeneity of variances for relative mRNA levels of *Rnd3* in human placentas.

Figure S3

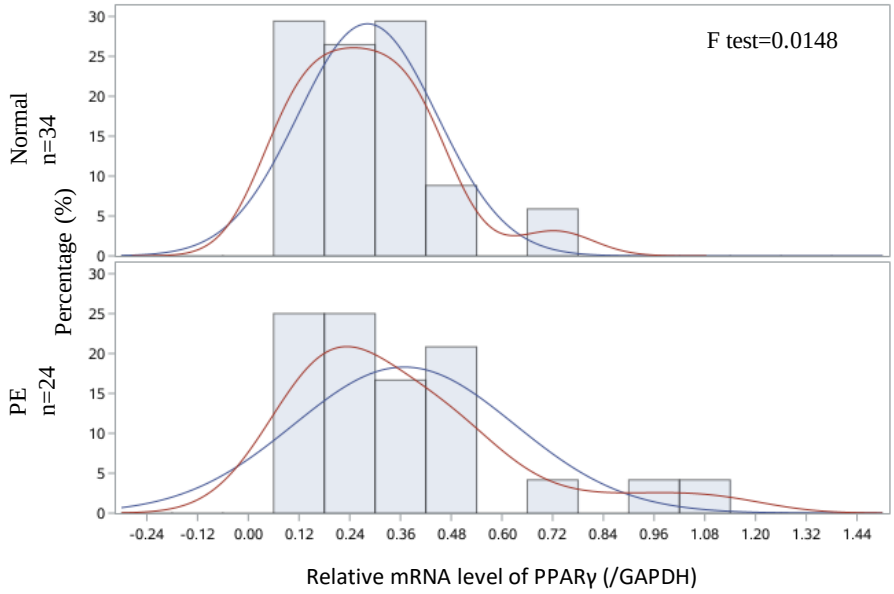

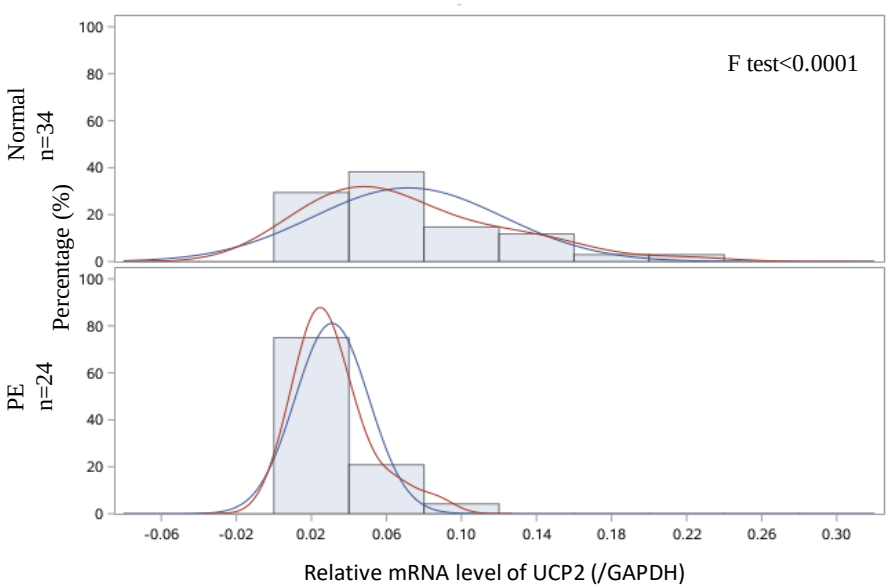

Figure S3. Tests of homogeneity of variances for relative mRNA levels of *PPARγ* and *UCP2* in human placentas.